Author/s:
Ebrahimipour, SY;Khosravan, M;White, J;Fekri, S

Title:
Preparation, crystal structure, spectroscopic studies, DFT calculations, antibacterial activities and molecular docking of a tridentate Schiff base ligand and its cis-MoO2 complex

Date:
2018-04-01

Citation:
Ebrahimipour, S. Y., Khosravan, M., White, J. & Fekri, S. (2018). Preparation, crystal structure, spectroscopic studies, DFT calculations, antibacterial activities and molecular docking of a tridentate Schiff base ligand and its cis-MoO2 complex. Applied Organometallic Chemistry, 32 (4), https://doi.org/10.1002/aoc.4233.

Ebrahimipour S. Yousef (Orcid ID: 0000-0002-6550-9452)

Preparation, crystal structure, spectroscopic studies, DFT calculations, antibacterial activities and molecular docking of a tridentate Schiff base ligand and its *cis*-MoO_2 complex

S. Yousef Ebrahimipour*[,1], Mehrji Khosravan[1], Jonathan White[2], Sahar Fekri[1]

[1] Department of Chemistry, Faculty of Science, Shahid Bahonar university of Kerman, Kerman, Iran

[2] School of Chemistry and Bio-21 Institute, University of Melbourne, Australia

Corresponding author:

Dr. S. Yousef Ebrahimipour

This is the author manuscript accepted for publication and has undergone full peer review but has not been through the copyediting, typesetting, pagination and proofreading process, which may lead to differences between this version and the Version of Record. Please cite this article as doi: 10.1002/aoc.4233

Department of Chemistry, Faculty of Science

Shahid Bahonar University of Kerman

76169-14111, Kerman, Iran

Tel/fax: +98 34 3132 2143

E-mails addresses: Ebrahimipour@uk.ac.ir, Ebrahimipour@ymail.com

Abstract

We synthesized a tridentate Schiff base ligand, 6-(((2-hydroxyphenyl)amino)methylene)-2-methoxycyclohexa-2,4-dienone [H_2L], as well as its Mo(VI) complex [MoO_2(L)(DMSO)], and then characterized them completely using elemental analysis, FT-IR , UV–Vis and ^{1}HNMR spectroscopy techniques. X-ray single crystal diffraction method was used for the determination of the structure of the synthesized ligand and complex. All other spectroscopic techniques performed, confirmed that [MoO_2(L)(DMSO)]had an octahedral geometry around the Mo(VI) central ion coordinated by the donor atoms of the deprotonated ligand, two oxido groups and one oxygen atom of DMSO molecule. Hybrid functional B3LYP with DGDZVP as basis set was applied for DFT calculations of the compounds in their ground state. The MEP, Mulliken, HOMO-LUMO energy gap and thermodynamic properties of the compounds were also theoretically predicted. In-vitro antimicrobial studies on the synthesized compounds indicated the great antibacterial activities of the Mo(VI) complex against *Escherichia coli*, *Staphylococcus aureus*, *Pseudomonas aeruginosa* and *Bacillus cereus* bacteria.

Keywords: *Cis*-MoO_2 complex, ONO Schiff base, X-ray crystal structure, Antimicrobial activity, Molecular docking, DFT Calculation

1 Introduction

Molybdenum (Mo) is a transition metal existing in a wide range of metalloenzymes and so, has biological importance in different living organisms such as bacteria, fungi, algae, plants and animals [1].

Various Schiff base complexes of Mo have been synthesized using the ability of this metal to form stable complexes with the ligands containing different donor atoms [2]. Biological activities of the Mo complexes especially *cis*-dioxomolybdenum(VI) complexes, have been widely studied. For example, these complexes have been demonstrated to act as models for the active sites of oxo-transfer molybdoenzymes [3]. Additionally, other properties including antimicrobial activities of them have also been reported [4].

To survey the antimicrobial activity of a potent agent, different strategies have been introduced. Among them, investigation of the influence of the agent on glucosamine-6-phosphate synthase (GlcN-6-P synthase) has been extensively considered in antimicrobial studies [5-6]. GlcN-6-P synthase produces GlcN-6-P which is vital for the pathogenic cells. So, inactivation of this enzyme is lethal for the microorganism [7]. This inactivation and subsequent antimicrobial activity can be studied theoretically using molecular docking [8-9].

Although the biological activities of Mo compounds have been demonstrated, their antibacterial properties have not been studied widely. In continuation of our research on biologically active species [10-12], we synthesized an ONO donor Schiff base, 2-(((2-hydroxyphenyl)imino)methyl)-6-methoxyphenol (H_2L), and its dioxo-molybdenium(VI) complex, [MoO_2(L)(DMSO)]. After full characterization of the title molecules, DFT calculations were also performed at B3LYP/DGDZVP level. Finally, the antimicrobial activities of the synthesized ligand and complex against various microorganisms were evaluated experimentally and theoretically.

2 Experimental

2.1 Chemicals and apparatus

All the chemical reagents utilized were of spectroscopic grade and used as received without further purification. Melting points were measured on an Electrothermal 9100 apparatus. Fourier transform infrared (FT-IR) spectra were recorded on a Schimadzu system FT-IR 8400

spectrophotometer using KBr pellets. ^{1}H NMR spectra were obtained with a Bruker Avance-300 MHz spectrometer using tetramethylsilane (TMS) as the internal standard. The ORTEP diagram numbering of the compounds used for the assignment of the protons resonances. A Cary 50 spectrophotometer was used to record the electronic spectra of the synthesized compounds (4×10^{-5} mol L^{-1} in EtOH) in the range of 200–800 nm.

2.2 Synthesis of 6-(((2-hydroxyphenyl)amino)methylene)-2-methoxycyclohexa-2,4-dienone [H_2L] (1)

An ethanolic solution (3 ml) containing 1 mmol 2-amino phenol (0.11 g) was added to equimolar amount of 3-methoxysalicylaldehyde (0.15 g) dissolved in 3 ml ethanol. The obtained mixture was then stirred for 5 min. An orange precipitate was formed that was separated after filtration, washed with cold ethanol, and dried in a desiccator over anhydrous $CaCl_2$. After slow evaporation of the solvent in ambient condition for 3 days, orange crystal suitable for crystallography were obtained.

Yield: 85%. m.p.=194^{o}C, Elemental Anal. $C_{14}H_{13}NO_3$ (243.25): Calc.: C, 69.12; H, 5.39; N, 5.76. Found: C, 69.10; H, 5.43; N, 5.71. FT-IR (KBr, cm^{-1}):ν(O-H): 3424, ν(N-H): 3054, ν(C=O):1667, ν(C=N):1632, ν(C=C):1499, ν(C-O):1306., ^{1}H-NMR (300 MHz, DMSO-d_6, 25 ºC, ppm): δ = 14.1 (s, 1H; $O^{1}H$; Exchange with D_2O), 9.9 (s, 1H; $O^{3}H$; Exchange with D_2O), 9.1 (s, 1H, $C^{7}H{=}N^{1}$), 6.9-7.5 (m, 7H, H^{4}-H^{6} and H^{10}-H^{13}) 3.91(s, 3H, $O^{2}C^{14}H_3$).UV/Vis (EtOH) λ_{max}, nm (ε, L mol^{-1} cm^{-1}): 233 (54954), 330 (19055), 445 (2754)

2.3 Synthesis of *Cis*-dioxo-dimethylsulfoxide-2-methoxy-6-(((2-oxidophenyl)imino)methyl) phenolate-molybdenum(VI) [MoO_2(L)(DMSO)] (2)

A DMSO solution (4 mL) containing 0.1 mmol H_2L (0.02 g) and 0.1 mmol $MoO_2(acac)_2$ (0.04 g) was stirred at room temperature for 10 min. After slow evaporation of the solvent in ambient condition for 2 days, red crystals suitable for X-ray analysis were obtained. The obtained red crystals were filtered off and dried in a desiccator over anhydrous $CaCl_2$.

Yield: 72%. m.p.: >300 °C. Molar conductance (10^{-3} M, DMSO): 8.0 Ω^{-1} cm^2 $mol^{-1,}$ Elemental Anal. $C_{16}H_{17}MoNO_6S$ (447.33): Calc.: C,42.96; H,3.83; N,3.13. Found: C,42.98; H,3.73; N,3.11. FT-IR (KBr, cm^{-1}): ν(C=N):1613, ν(C=C):1490, ν(C-O):1285, $\nu(MoO_2)$: 899 and 999. ^{1}H-NMR (100 MHz, DMSO-d_6, 25 ^{o}C, ppm): δ= 9.43 (s, 1H, $C^7H{=}N^1$), 7.01-8.0 (m, 7H, H^4-H^6 and H^{10}-H^{13}), 3.97 (s, 3H, $O^2C^{14}H_3$), 2.4 (s, 6H, $S^1(CH_3)_2$). UV/Vis (EtOH) λ_{max}, nm (ε, L mol^{-1} cm^{-1}): 235 (69183), 310 (22909), 365 (9772), 425 (5129)

2.4 Crystal structure determination

Intensity data for **[**H_2L] and [MoO_2(L)(DMSO)] were collected at 100 K on the MX1 beamline [13] at the Australian Synchrotron. The structures were solved by direct methods and difference Fourier synthesis [14]. Thermal ellipsoid plots were generated using the program ORTEP-3 [15] integrated within the WINGX suite [16] of programs. Details of crystal data and structural refinement are given in Table 1.

2.5 DFT calculation

Full geometry optimization of the complex in ground state (S_0) was performed using DFT-B3LYP with DGDZVP basis set using the G03 program [17]. Crystal structure of [H_2L] and [MoO_2(L)(DMSO)] were used as the starting point of the calculations. Frequency calculations at the same levels of theory disclosed no imaginary frequencies, indicating that an optimal geometry at these levels of approximation was found for the compounds.

2.6 Biological activity

To evaluate the antimicrobial activity of [H_2L] and [MoO_2(L)(DMSO)], agar well diffusion method and minimum inhibitory concentration (MIC) were used. *Escherichia coli*, *Staphylococcus aureus*, *Pseudomonas aeruginosa* and *Bacillus cereus* bacteria studied here were grown overnight and then suspended in Muller Hinton broth to match the 0.5 McFarland standards [18]. In the well diffusion method, the inoculums suspension of the microbial stains was swabbed on the entire surface of the agar media. Wells were made and then 50 µl of each compound at two different concentrations (500 µg/ml and1000 µg/ml) was added to each well. The plates were incubated at 37°C for 24-48 h. Antimicrobial activity was assayed by measuring the diameter of the inhibition zone (IZ) formed around the wells in millimetre (mm). DMSO (as the solvent) was used as a negative control, whereas azithromycin (a standard antibiotic) were used as positive control [18]. MIC is defined as the lowest concentration of a typical compound

or drug that completely inhibit the growth of a given strain. The values of MIC for the ligand and its Mo(VI) complex were calculated accordingly. Serial two-fold dilution (from 1000 µM to 7.8 µM) for the ligand and the Mo(VI) complex in DMSO were carried out in the agar media. Overnight broth culture of *E. coli*, *S. aureus*, *P. aeruginosa* and *B. cereus* were prepared with bacteria suspension (make $\frac{1}{140}$ dilution of the 0.5 McFarland turbidity). The assay was performed in nutrient broth for bacteria. The plates were incubated at 37 °C under suitable conditions depending upon the test microorganism. Finally, the turbidity of the wells was measured using a micro plate reader device. Growth of the microorganisms was followed by monitoring the absorbance at 620 nm after 24 h until the stationary phase was reached [8].

2.7 Molecular docking

Crystal structure of GlcN-6-P synthase was obtained from the Protein Data Bank (http://www.pdb.org/pdb/home/home.do), PDB ID 2VF5, at a resolution of 2.90 Å. The binding site of the target was selected based on the amino acid residues involved in binding to the glucosamine-6-phosphate of GlcN-6-P synthase as obtained from PDB with ID 2VF5 which would be considered the best accurate active region solved by experimental crystallographic data. The grid was accordingly centred at the region including all the 12 amino acid residues surrounding the active site (Ala602, Val399, Ala40 0, Gly301, Thr302, Ser303, Cys300, Gln348, Ser349, Thr352, Ser347 and Lys603). The coordination spheres of the complex was generated from its X-ray crystal structure as a CIF file. The CIF file was then converted to PDB format

using Mercury software (http://www.ccdc.cam.ac.uk/). Finally, molecular docking studies were carried out using Autodock 4.2.5 software [19] with the grid box size set at 70, 64, and 56 A° for x, y and z, respectively. The grid centre was set at 30.59, 15.822 and 3.497 for x, y and z, respectively. Discovery Studio Visualizer 4.5 package was used to produce the molecular images and animations.

3 Results and discussion

3.1 Spectral characterizations

3.1.1 FT-IR

FT-IR spectra of the free ligand H_2L and its Mo(VI) complex were recorded and compared with each other. In the spectrum of the ligand, O-H and N-H stretching vibrations were appeared at 3424 and 3054 cm^{-1}, respectively [20]. Absorption band corresponding to C=O (1667 cm^{-1}) was observed in the free ligand spectrum suggesting the *keto* form of the ligand in its free form. However, this peak was absent in the spectrum of the complex indicating the complexation process. Stretching vibration of C=N was appeared as a strong band at 1632 cm^{-1} in the spectrum of the free ligand while in the complex spectrum, this peak showed a red shift of 19 cm^{-1} due to the coordination of the azomethine nitrogen atom to the Mo(VI) ion [21]. Additionally, the blue shift observed in the ν(C-O) from 1306 cm^{-1} in the free ligand to 1285 cm^{-1} in the complex was an evidence for the coordination of the ligand to the metal ion through the phenolic oxygen atom

[22]. Two strong bands at 899 and 999 cm^{-1} were respectively assigned to the symmetrical and asymmetrical ν (O=Mo=O) of the dioxidomolybdenum(VI) complex [23].

3.1.2 ^{1}HNMR study

As we reported previously [10-11], H_2L and similar structures have two tautomeric forms namely *keto* and *enol* forms. The former is the most stable structure in solid state and the latter is the most stable structure in solution.

In the ^{1}H NMR spectrum of the ligand, the singlet signals appeared at 14.1 and 9.9 ppm were assigned to aldehyde O-H and amine OH, respectively. Coordination of these groups to the Mo(VI) ion resulted in the disappearance of these signals in the spectrum of the complex. A down-field shift was observed in the signal of the azomethine proton of the Mo(VI) complex (9.1 ppm) indicating compared with that of the free ligand spectrum (9.43 ppm), demonstrating the formation of metal–nitrogen bond. In the ^{1}H NMR spectrum of the complex, the signals appeared at 3.97 and 2.4 ppm were assigned to protons of the methoxy and methyl moieties, respectively. Protons of the rings were observed as multiplet signals at 6.9-7.5 ppm in the free ligand spectrum and at 7.01-8 ppm in the complex spectrum.

3.1.3 Electronic spectra

Electronic spectra of the synthesized compounds were recorded in ethanol (Table 2). In the spectrum of the free ligand, $\pi \rightarrow \pi^*$ transitions of the aromatic rings were appeared at 233 nm.

The absorption bands at 330 nm and 445 nm were assigned respectively to the π→π* and n→π* transitions of the azomethine moiety [11]. Similar features were observed for the Mo(VI) complex. In addition, LMCT (O(*p*) →Mo(*d*)) transition resulted in an absorption peak at 425 nm. Since the Mo(VI) ion had d^0 electronic configuration (formal oxidation state of +6), no *d-d* transition was observed in the complex spectrum.

3.2 X-ray crystal structure

A thermal ellipsoid plot for H_2L is presented in Figure 1, and selected bond distances are given in Table 3. [H_2L] adopts the tautomeric form (A) in the solid state (Figure 2), with significant contributions of the zwitterionic resonance form (A') being evident from inspection of the appropriate bond distances which are given in Table 3. This structure is stabilized by intramolecular resonance-assisted N-H…O hydrogen bonding [24]. The two aromatic rings and the imine double bond are essentially co-planar (RMS deviation 0.0237 Å), while the methoxyl substituent is also coplanar with the aromatic ring defined by atoms C1-C6; (C14-O2-C3-C4 -4.2(2)°) a conformation which allows for delocalization of the p-type lone pair into the aromatic ring.

The molecules of [H_2L] form intermolecular H-bonded chains, which extend along the b-direction of the crystal (Figure 3). H-bond parameters; (O3-H…O1; O3…O1 2.60(1) Å, O3-H…O1 = 170(2)° with symmetry code (1-x, 0.5-y, 0.5-z). Alternate members of this H-bonded chain are close to orthogonal with one another with an interplanar angle 84.94(3)°. The H-

bonded chains are interdigitated by π-stacking interactions with parallel inversion related H-bonded chains (symmetry code (1-x,-y,1-z) (Figure 4). The π-stacking interactions are characterized by an interplanar distance of 3.244(2) Å and a slippage distance of approximately 2.679 Å. The molybdenum complex, $[MoO_2(L)(DMSO)]$, derived from the ligand (H_2L) crystallises with two molecules in the asymmetric unit (Figure 1) Superposition of these two molecules reveals differences in the orientation of the coordinated DMSO molecule with respect to the ligand, but otherwise they are very similar (Figure 5). Selected bond distances for this complex are listed in Table 4. The coordinated ligand in both molecules adopts essentially the same conformation as the free ligand (H_2L), the π-systems in both molecules are coplanar with RMS deviations for the two molecules being 0.0412 and 0.0206 Å respectively. The bond distances in the coordinated ligand compare qualitatively with those in the free ligand but with greater contributions of the resonance form similar to A' (where N-H) is replaced with N-Mo. The Mo metal in both molecules adopts a slightly distorted octahedral geometry which compare with similar complexes present in the Cambridge Crystallographic Database.

3.3 Geometry Optimization

To determine the electronic structure of the synthesized compounds in more details, B3LYP correlation function by the Gaussian 03 package using a DFT method was performed. Tables 3 and 4 give the selected geometrical parameters. As one can see, the optimized bond lengths and

angles for the ligand and its Mo(VI) complex are in good agreement with those obtained from the experimental structure data (single crystal X-ray diffraction). However, minor deviations are observed originated from the fact that the theoretical calculations have been carried out for an isolated molecule in gas phase while the experimental XRD results have been obtained in solid state. Figure 6 reveals the molecular structures of H_2L and its Mo(VI) complex obtained from Gaussian 03W and GaussView 5.0 programs.

3.4 Charge distribution and electronic structure

The atomic charge value calculated for the Mo(VI) central ion was considerably lower than that expected considering the formal charge of +6. This was due to the significant electron transition from the ligand to the Mo(VI) central ion (Table 5). Moreover, study of the charge values and valance electron configuration of the donor atoms confirmed this difference. Mullikan charge value calculated for the donor atoms was also less than that predicted; it was another evidence for charge donation from the ligand to the metal ion.

Chemical reactivity and some of the physical properties of a typical molecule can be found from its Frontier Molecular Orbitals (FMO) [25]. Figure 7 depicts the energy level of the molecular orbitals with isodensity surface plots of the highest occupied molecular orbital (HOMO) and the lowest unoccupied molecular orbital (LUMO) of the synthesized ligand and $[MoO_2(L)(DMSO)]$ complex. It is well known that the HOMO is responsible for electron donating ability of a compound while electron accepting is related to LUMO. Moreover, the stability of structures can be determined using the energy gap between HOMO and LUMO. This gap also can be used to characterize some

important features, including the kinetic stability and chemical reactivity of the molecule. It has been demonstrated that small frontier orbital space of a typical compound is responsible to its low kinetic stability and high chemical reactivity [26]. The values of the band gap for H_2L and Mo(VI) complex were found to be 3.00 and 2.98 eV, respectively. Thus, the complex had a higher chemical reactivity compared with the Schiff base ligand. It was also found that in the title Mo(VI) complex, the Schiff base ligand had more contribution to the HOMO while the LUMO was mainly localized on the central Mo(VI) ion. Accordingly, the first transition from the HOMO to the LUMO in the Mo(VI) complex was attributed to ligand-metal charge transfer (LMCT).

3.5 Thermodynamic properties

Thermodynamic properties of the ligand (1) and its Mo(VI) complex (2) were also predicted using DFT calculations. To do this, standard thermodynamic functions including enthalpy (H_m^0), entropy (S_m^0) and heat capacity $(C_{p,m}^0)$ of the title compounds at different temperatures were calculated at DFT/B3LYP. According to the obtained results given in Table 6, when the temperature increased from 200 K to 800 K, the thermodynamic values increased as a result of increasing the vibrational intensities. The equations correlating enthalpy, entropy and heat capacity of the compounds to temperature are as follows:

$H_m^\circ(1) = 0.00007T^2 + 0.0231T + 150.26$ ($R^2 = 0.9998$)

$C_{p,m}^\circ(1) = -0.0001T^2 + 0.2561T - 4.192$ ($R^2 = 0.9999$)

$S_m^\circ(1) = -0.000005T^2 + 0.2455T + 60.446$ ($R^2 = 1$)

$H_m^\circ(2) = 0.00009T^2 + 0.0457T + 189.52$ ($R^2 = 0.9999$)

$C_{p,m}^\circ(2) = -0.0002T^2 + 0.3415T + 7.7374$ ($R^2 = 0.9999$)

$S_m^\circ(2) = -0.0001T^2 + 0.388T + 68.661$ ($R^2 = 1$)

3.6 Molecular electrostatic potential

Molecular electrostatic potential (MEP) depicts the shape, size, and simultaneously the electrostatic potential of a typical molecule using colour grading. Figure 8 shows the MEP of the synthesized ligand and complex. Different colours in the figure represent different values of the electrostatic potential. Regions with the most negative electrostatic potential have been shown in red. Blue and green have been used to represent regions with the most positive electrostatic potential and zero potential, respectively. Briefly, the electrostatic potential increases in the order red < orange < yellow < green < cyan < blue. According to Figure 8, oxygen of the aldehyde moiety is the electron-rich area in the structure of the ligand while in the complex, the oxido groups and the oxygen of the amine ring make the electron-rich region. The electropositive sites are the OH moieties of the amine ring in the ligand, and the coordinated solvent and the nitrogen of the azomethine group in the complex.

3.7 Antibacterial activity

To evaluate the antibacterial activity of H_2L and $[MoO_2(L)(DMSO)]$, inhibition zone (IZ) and MIC values for each compound against some Gram-positive and Gram-negative bacteria namely *Escherichia coli, Staphylococcus aureus, Pseudomonas aeruginosa* and *Bacillus cereus* were measured. Table 7 gives the values of IZ obtained for the synthesized compounds at two concentrations (500 and 1000 µg/ml) as well as those obtained for the positive and negative controls. As can be seen, the highest antibacterial activity against all studied microorganisms was attributed to $[MoO_2(L)(DMSO)]$. Surprisingly, the title complex and its parent ligand showed considerable antibacterial activity against *P. aeruginosa* while this species was resistant to the antibiotic azithromycin. Consequently, the synthesized Mo(VI) complex was effective on both Gram-negative and Gram-positive bacteria. The MIC values measured for H_2L and $[MoO_2(L)(DMSO)]$ are reported in Table 8. As one can see, the MIC values of the ligand against the tested bacteria were in the range of 15.63-62.5 µM while those of the complex were in the range of 7.8-62.5 µM. These data revealed the higher antimicrobial activity of the complex.

Using chelation theory [27], we can describe the enhanced antimicrobial activity of the complex relative to the ligand. Five parameters have been demonstrated to influence on the antimicrobial property of a typical metal complex; these parameters are chelate effect, nature of the coordinating groups, total charge of the complex, nature of the counter ion in ionic complexes and nuclearity of the central metal ion [28]. Tweedy's chelation theory states that partial sharing of the positive charge of the metal ion with donor atoms of the ligands as a result of complexation decreases the polarity of the metal ion [11]. On the other side, according to

Overtone's concept the lipophilicity of the complex is generally higher than that of the free ligand due to the delocalization of π-electrons over the whole complex structure. Consequently, the penetration of the complex into the lipid membranes of the microorganisms is improved [11]. Moreover, respiration process of the microorganism cells has been reported that can be affected by metal complexes. Hence, the synthesis of proteins is disturbed and further growth of the microorganism is restricted [29].

3.8 Molecular docking

The results of molecular docking confirmed those of the antimicrobial experiments. As shown in Figure 9, [MoO_2(L)(DMSO)] bound to the active site of GlcN-6-P synthase via one or more amino acids. Also, the value of theoretical binding energy was calculated for the tested compounds ([MoO_2(L)(DMSO)] and azithromycin). The binding energy of [MoO_2(L)(DMSO)]-enzyme system (-4.63 kcal/mol) was higher than those of azithromycin-enzyme (-4.27 kcal/mol) suggesting that the synthesized Mo(VI) complex had more inhibitory effect on GlcN-6-P synthase. These data were in good agreement with the experimental results. Consequently, [MoO_2(L)(DMSO)] may be introduced as a good antimicrobial agent.

4 Conclusions

A tridentate Schiff base ligand [H_2L] and its Mo(VI) complex has been synthesized and characterized using physico-chemical and spectroscopic methods including spectroscopy

techniques. Single crystal X-ray diffraction data reveal that the Mo(VI) ion is surrounded by ONO donor atoms of L^{2-}, two oxido groups and oxygen of the coordinated solvent (DMSO).The results of DFT calculations in gas phase were in a good accordance with those obtained experimentally. Since the HOMO–LUMO energy gap of the complex is larger than that of the ligand, it is expected that the complex has a higher chemical reactivity compared with the Schiff base ligand. Using molecular electrostatic potential (MEP), one can find that the electropositive sites are the OH moieties of the amine ring in the ligand and the coordinated solvent and the nitrogen of the azomethine group in the complex, while electron-rich regions are oxygen of the aldehyde moiety in the ligand and the oxido groups and the oxygen of the amine ring in the complex. According to the thermodynamic studies, increasing the temperature increases the vibrational intensities in both compounds. Both experimental and theoretical studies indicate higher antimicrobial activity of the $[MoO_2(L)(DMSO)]$ complex compared with its parent ligand as well as the antibiotic azithromycin.

Supplementary data

CCDC 1529697 and 1529698 contain the supplementary crystallographic data for H_2L and $[MoO_2(L)(DMSO)]$. These data can be obtained free of charge via http://www.ccdc.cam.ac.uk/conts/retrieving.html, or from the Cambridge Crystallographic Data Centre, 12 UnionRoad, Cambridge CB2 1EZ, UK; fax: (+44) 1223-336-033, or e-mail: deposit@ccdc.cam.ac.uk, web page: http://www.ccdc.cam.ac.uk/cgibin/catreq.cgi

Acknowledgements

Authors gratefully acknowledge the financial support of the Shahid Bahonar University of Kerman.

References

[1] I. Bertini, Biological inorganic chemistry: structure and reactivity, University Science Books, 2007.

[2] a) M. R. Maurya, L. Rana, N. Jangra, F. Avecilla, Chem. Select 2(23) (2017) 6767-6777; b) A. Bezaatpour, E. Askarizadeh, S. Akbarpour, M. Amiria, B. Babaei, Mol. Catal. 436 (2017)199-209; c) A. M. Fayed, S. A. Elsayed, A. M. El-Hendawy, M. R. Mostafa, Spectrochim. Acta A 129 (2014) 293-302.

[3] a) J. T. Spence, Coord. Chem. Rev. 48(1) (1983) 59-82 ; b) B. K. Burgess, D. J. Lowe, Chem. Rev. 96(7) (1996) 2983-3012; c) R. Hille, Chem. Rev. 96(7) (1996) 2757-2816.

[4] a) S.P. Sovilj, D. Mitić, B.J. Drakulić, M. Milenković, J. Serb. Chem. Soc. 77 (1) (2012) 53–66; b) Z. Asgharpour, F. Farzaneh, M. Chiasi, M. Azarkish,Appl. Organomet. Chem, 31(11) (2017) e3782; c) S. Pasayat, S. P. Dash, Saswati, P. K. Majhi, Y. P. Patil, M. Nethaji, H. R. Dash, S. T. Das, R. Dinda, Polyhedron 38(1) (2012) 198-204; d) E.K. Efthimiadou, Y. Sanakis, N. Katsaros, A. Karaliota, G. Psomas, Polyhedron, 26 (2007) 1148-1158.

[5] S. Milewski, Biochim. Biophys. Acta (BBA)-Protein Struct. Mol. Enzymol. 1597 (2002) 173-192.

[6] S.Y. Ebrahimipour, I. Sheikhshoaie, J. Castro, M. Dušek, Z. Tohidiyan, V. Eigner, M. Khaleghi, RSC Adv. 5 (2015) 95104-95117.

[7] P. Shyma, B. Kalluraya, S. Peethambar, S. Telkar, T. Arulmoli, Eur. J. Med. Chem. 68 (2013) 394-404.

[8] F. Heidari, S.J.A. Fatemi, S.Y. Ebrahimipour, H. Ebrahimnejad, J. Castro, M. Dušek, V. Eigner, Inorg. Chem. Commun. 76 (2017) 1-4.

[9] G. Jose, T.S. Kumara, G. Nagendrappa, H. Sowmya, J.P. Jasinski, S.P. Millikan, N. Chandrika, S.S. More, B. Harish, Eur. J. Med. Chem. 77 (2014) 288-297.

[10] a) S.Y. Ebrahimipour, M. Mohamadi, J. Castro, N. Mollania, H.A. Rudbari, A. Saccá, J. Coord. Chem. 68 (2015) 632-649; b) S.Y. Ebrahimipour, M. Mohamadi, M. Torkzadeh Mahani, J. Simpson, I. Sheikhshoaei, Eur. J. Med. Chem. 140 (2017) 172-186.

[11] R. Takjoo, A. Akbari, S.Y. Ebrahimipour, M. Kubicki, M. Mohamadi, N. Mollania, Inorg. Chim. Acta, 455 (2017) 173-182.

[12] S.Y. Ebrahimipour, I. Sheikhshoaie, A. Crochet, M. Khaleghi, K.M. Fromm, J. Mol. Struct., 1072 (2014) 267-276.

[13] Cowieson, N.P., D. Aragao, M. Clift, D.J. Ericsson, C. Gee, S.J. Harrop, N. Mudie, S. Panjikar, J.R. Price, and A. Riboldi-Tunnicliffe, J. Synchrotron Radiat. 22(1) (2015) 187-190.

[14] Sheldrick, G.M., Acta Crystallogr.C 71(1) (2015) 3-8.

[15] Farrugia, L.J., J. Appl. Crystallogr. 30(5) (1997) 565-565.

[16] Farrugia, L.J., J. Appl. Crystallogr. 45(4) (2012) 849-854.

[17] Gaussian 03, Revision C.02, M.J. Frisch, G.W. Trucks, H.B. Schlegel, G.E. Scuseria, M.A. Robb, J.R. Cheeseman, J.A. Montgomery, Jr., T. Vreven, K.N. Kudin, J.C. Burant, J.M. Millam, S.S. Iyengar, J. Tomasi, V. Barone, B. Mennucci, M. Cossi, G. Scalmani, N. Rega, G.A. Petersson, H. Nakatsuji, M. Hada, M. Ehara, K. Toyota, R. Fukuda, J. Hasegawa, M. Ishida, T. Nakajima, Y. Honda, O. Kitao, H. Nakai, M. Klene, X. Li, J.E. Knox, H.P. Hratchian, J.B. Cross, V. Bakken, C. Adamo, J. Jaramillo, R. Gomperts, R.E. Stratmann, O. Yazyev, A.J. Austin, R. Cammi, C. Pomelli, J.W. Ochterski, P.Y. Ayala, K. Morokuma, G.A. Voth, P. Salvador, J.J. Dannenberg, V.G. Zakrzewski, S. Dapprich, A.D. Daniels, M.C. Strain, O. Farkas, D.K. Malick, A. D. Rabuck, K. Raghavachari, J.B. Foresman, J.V. Ortiz, Q. Cui, A.G. Baboul, S. Clifford, J.

Cioslowski, B.B. Stefanov, G. Liu, A. Liashenko, P. Piskorz, I. Komaromi, R.L. Martin, D.J. Fox, T. Keith, M.A. Al-Laham, C.Y. Peng, A. Nanayakkara, M. Challacombe, P.M.W. Gill, B. Johnson, W. Chen, M.W. Wong, C. Gonzalez, J.A. Pople, Gaussian, Inc., Wallingford CT, 2004.

[18] Ebrahimipour, S.Y., I. Sheikhshoaie, J. Simpson, H. Ebrahimnejad, M. Dusek, N. Kharazmi, and V. Eigner, New J. Chem. 40(3) (2016) 2401-2412.

[19] Morris, G.M., R. Huey, W. Lindstrom, M.F. Sanner, R.K. Belew, D.S. Goodsell, and A.J. Olson, J. Comput. Chem. 30(16) (2009) 2785-2791.

[20] M. Mohamadi, S.Y. Ebrahimipour, J. Castro, M. Torkzadeh-Mahani, J. Photochem. Photobiol. B, 158 (2016) 219-227.

[21] M. Mohamadi, E. Faghih-Mirzaei, S.Y. Ebrahimipour, I. Sheikhshoaie, W. Haase, S. Foro, J. Mol. Struct. 1139 (2017) 418-429.

[22] R. Takjoo, A. Akbari, S.Y. Ebrahimipour, H.A. Rrudbari, G. Brunò, C. R. Chimie, 17 (2014) 1144-1153.

[23] I. Sheikhshoaie, S.Y. Ebrahimipour, S. Shamsi, Synth. React. Inorg. Met. Org. Chem., 46 (2016) 917-921.

[24] a) G. Gilli, F. Bellucci, V. Ferretti, V. Bertolasi, J. Am. Chem. Soc. 111 (1989) 1023-1028; b) T. Zych, T. Misiaszek, M.M. Szostak, Chem. Phys. 340 (2007) 260-272; c) I.V. Omelchenko, O.V. Shishkin, L. Gorb, F.C. Hill, J. Leszczynski, Struct. Chem. 23 (2012) 1585-1597; d) D.-C. Zhang, Y.-Q. Zhang, J. Energ. Mater. 15 (1997) 205-216.

[25] I. Sheikhshoaie, S.Y. Ebrahimipour, M. Sheikhshoaie, H.A. Rudbari, M. Khaleghi, G. Bruno, Spectrochim. Acta A 124 (2014) 548-555.

[26] J. Aihara, J. Phys. Chem. A, 103 (1999) 7487-7495.

[27] P.K. Panchal, H.M. Parekh, P.B. Pansuriya, M.N. Patel, J. Enzyme Inhib. Med. Chem. 21 (2006) 203-209.

[28] C. Dendrinou-Samara, G. Psomas, C.P. Raptopoulou, D.P. Kessissoglou, J. Inorg. Biochem. 83 (2001) 7-16.

[29] M. Imran, J. Iqbal, S. Iqbal, N. Ijaz, Turk. J. Biology, 31 (2007) 67-72.

Figure Captions

Figure 1. Thermal ellipsoid plots of H_2L(left) and [MoO_2(L)(DMSO)](right). Ellipsoids are at the 30% probability level.

Figure 2. Tautomeric form adopted by H_2L in the solid state.

Figure 3. H-bonded chains of [H_2L] extending along the b-axis of the crystal

Figure 4. (a) π-stacking between inversion related molecules of H_2L, (b) interdigitation between parallel H-bonded chains of H_2L

Figure 5. Overlay of the two independent molecules of [MoO_2(L)(DMSO)]

Figure 6. The optimized geometries of the H_2L(left) and [MoO_2(L)(DMSO)] (right)

Figure 7. Diagram of Frontier molecular orbital energies of H_2L and its Mo(VI) complex

Figure 8. Molecular electrostatic potential map of H_2L (left) and [MoO_2(L)(DMSO)] (right).

Figure 9. The docked Mo(VI)complex in the active pocket of GlcN-6-P.

Table 1. Crystal data and structure refinement for $[H_2L]$ and $[MoO_2(L)(DMSO)]$

		$[H_2L]$	$[MoO_2(L)(DMSO)]$
Empirical formula		$C_{14}H_{13}NO_3$	$C_{16}H_{17}MoNO_6S$
Formula weight		243.25	447.30
Crystal system		Monoclinic	Triclinic
Space group		$P2_1/c$	P-1
Temperature (K)		100	100
Unit cell dimensions	a (Å)	10.323 (2)	6.7440 (13)
	b (Å)	8.7930 (18)	16.212 (3)
	c (Å)	12.633 (3)	16.825 (3)
α (°)		90	71.97 (3)
β (°)		95.21 (3)	86.18 (3)
γ (°)		90	80.92 (3)
V (Å^3)		1142.0 (4)	1727.0 (7)
Z		4	4
Density (calculated), Mg/m^3		1.415	1.720
Radiation type		Mo-Kα, λ = 0.71073 Å	Synchrotron, λ = 0.71073 Å
F(000)		512	904
μ (mm^{-1})		0.10	0.91
Crystal size (mm)		0.07 × 0.06 × 0.05	0.06 × 0.05 × 0.05
No. of measured, independent and observed [I > 2σ(I)] reflections		21730, 3230, 2971	30921, 8249, 7898
R_{int}		0.080	0.031
$(\sin\theta/\lambda)_{max}$ (Å^{-1})		0.705	0.685
R[$F^2 > 2\sigma(F^2)$], wR(F^2), S		0.056, 0.153, 1.07	0.036, 0.090, 1.10
No. of reflections		3230	8249
No. of parameters		172	457
$\Delta\rho_{max}$, $\Delta\rho_{min}$ (e Å^{-3})		0.58, −0.41	1.31, −1.01

Table 2. Electronic spectral components for ligand [H_2L] and its Mo(VI) complex in EtOH (nm)

[H_2L]	[MoO_2(L)(DMSO)]	Assignment
233	235	π→π*
330	310	π→π*
445	365	n→π*
-	425	LMCT

Table 3. Selected bond distances for [H_2L]

Bond length	Exp*.	Ca l c **	Bond length	Exp.	Ca l c .
C(1)-C(7)	1.4113(14)	1.396	C(11)-C(12)	1.3923(15)	1.397
C(1)-C(2)	1.4262(13)	1.421	C(14)-O(2)	1.4261(13)	1.422
C(2)-C(3)	1.4442(14)	1.470	C(1)-C(6)	1.4220(13)	1.429
C(3)-C(4)	1.3752(14)	1.374	C(2)-O(1)	1.2912(12)	1.277
C(5)-C(6)	1.3667(15)	1.366	C(3)-O(2)	1.3656(12)	1.362
C(8)-C(13)	1.3905(13)	1.401	C(4)-C(5)	1.4143(15)	1.421
C(8)-N(1)	1.4107(13)	1.409	C(7)-N(1)	1.3135(12)	1.321
C(9)-C(10)	1.3974(14)	1.396	C(8)-C(9)	1.4079(13)	1.412
C(10)-C(11)	1.3856(14)	1.389	C(9)-O(3)	1.3504(12)	1.361

*=Experimental, **=Calculated

Table 4. Selected geometries for $[MoO_2(L)(DMSO)]$

Bond length	Exp*.	Calc**	Bond angle	Exp.	Calc.
N(2)-Mo(2)	2.292(2)	2.302	O(11)-Mo(2)-O(12)	104.96(10)	104.95
O(7)-Mo(2)	1.9281(19)	1.939	O(11)-Mo(2)-O(7)	98.21(10)	98.02
O(10)-S(2)	1.527(2)	1.548	O(12)-Mo(2)-O(7)	101.88(9)	101.66
O(11)-Mo(2)	1.707(2)	1.726	O(11)-Mo(2)-O(9)	97.32(10)	99.52
O(9)-Mo(2)	1.976(2)	1.989	O(12)-Mo(2)-O(9)	96.83(9)	97.01
O(10)-Mo(2)	2.290(2)	2.313	O(7)-Mo(2)-O(9)	151.63(9)	149.33
O(12)-Mo(2)	1.716(2)	1.734	O(11)-Mo(2)-O(10)	166.95(8)	167.58
			O(9)-Mo(2)-N(2)	74.63(9)	73.93
			O(7)-Mo(2)-O(10)	77.14(9)	78.24
			O(7)-Mo(2)-N(2)	81.60(8)	80.13
			O(10)-Mo(2)-N(2)	76.70(8)	75.42

*=Experimental, **=Calculated

Table 5. Charges and electron configurations for [MoO_2(L)(DMSO)]

atom	Charge	Electron configuration
Mo	1.79192	[core]5S(0.21)4d(3.59)5p(0.42)5d(0.03)
O1	-0.67619	[core]2S(1.62)2p(4.92)3p(0.01)3d(0.01)
N1	-0.55890	[core]2S(1.34)2p(4.19)3p(0.02)
O3	-0.69110	[core]2S(1.67)2p(5.00)3p(0.01)
O4	-0.97492	[core]2S(1.82)2p(5.14)3p(0.01)3d(0.01)
O5	-0.51348	[core]2S(1.84)2p(4.67)3d(0.01)
O6	-0.58235	[core]2S(1.84)2p(4.73)3d(0.01)

Table 6. Thermodynamic properties of $[H_2L]$ and its Mo(VI) complex at different temperatures

Temperature (K)	Enthalpy (Kcal mol^{-1})		Entropy (cal mol^{-1} K^{-1})		Heat capacity (cal mol^{-1} K^{-1})	
	1	**2**	**1**	**2**	**1**	**2**
200	157.924	202.615	42.53	69.482	107.505	141.694
298.15	163.02	210.688	61.255	94.744	128.78	174.993
300	163.133	210.863	61.602	95.202	129.172	175.593
400	170.199	221.57	79.339	118.348	149.949	206.805
500	178.909	234.402	94.359	137.626	169.765	235.803
600	188.976	248.969	106.548	153.136	188.448	262.68
700	200.141	264.929	116.403	165.631	205.945	287.565
800	212.197	282.019	124.467	175.845	222.297	310.636

Table 7: Antimicrobial activities of the different amounts of compounds against gram-positive and gram-negative bacteria determined by the agar well diffusion method**.**

	$[H_2L]$		$[MoO_2(L)(DMSO)]$		Positive control	Negative control
	500 µg/ml	1000 µg/ml	500 µg/ml	1000 µg/ml	Azithromycin (15µg/ml)	DMSO
E. coli	20	27	22	29.1	25	-
S. aureus	9	11.3	11	15	25.5	-
B. cereus	10	14	12.6	17	20	-
P. aeruginosa	12.2	15.2	16.6	18.2	-	-

Table 8: The MIC values of [H_2L], [MoO_2(L)(DMSO)] and the negative control against microorganisms.

	E. coli	*S. aureus*	*B. cereus*	*P. aeruginosa*
[H_2L]	62.5	31.25	15.63	15.63
[MoO_2(L)(DMSO)]	15.63	7.8	7.8	15.63
Negative control (DMSO)	-	-	-	-

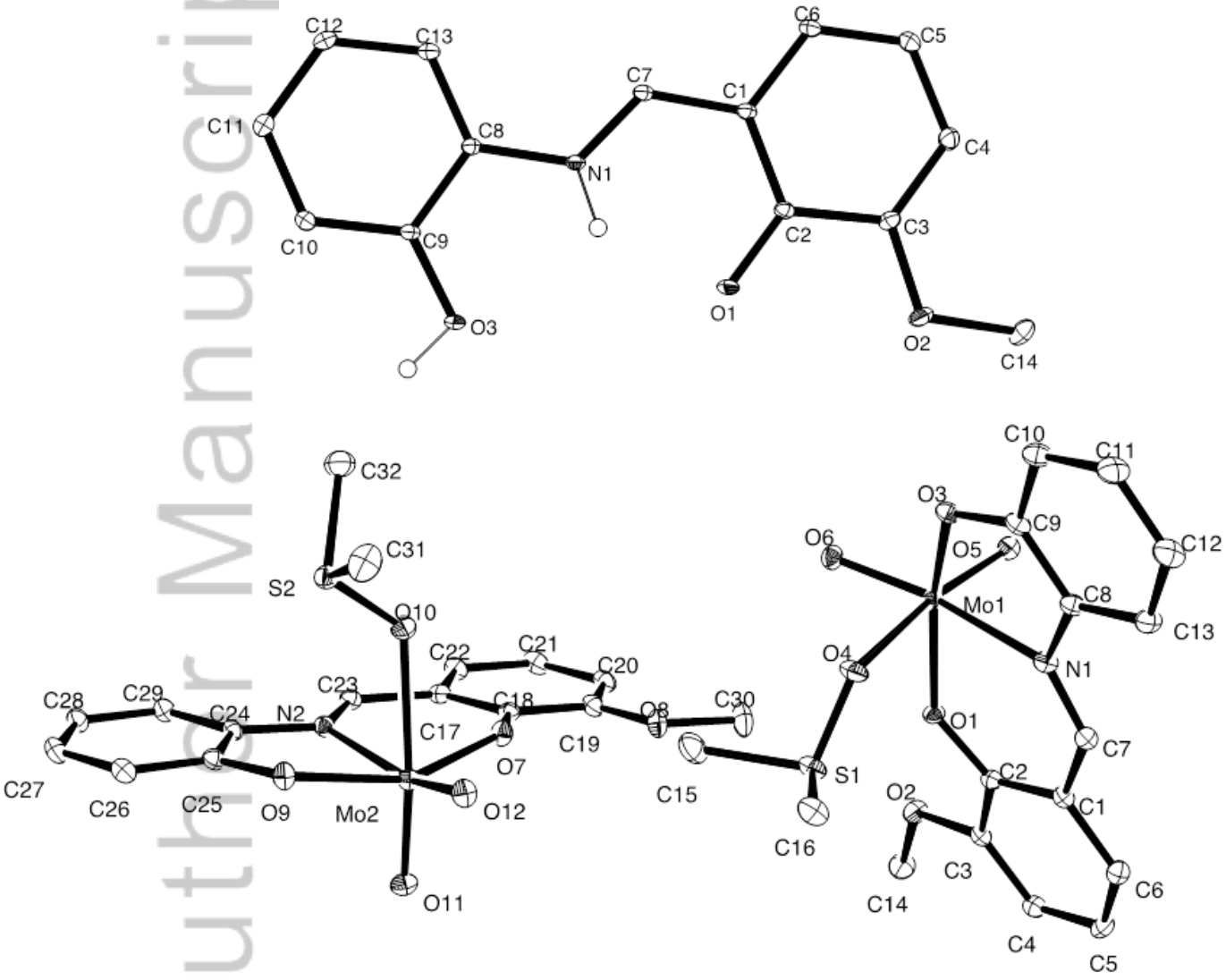

AOC_4233_F1.TIF

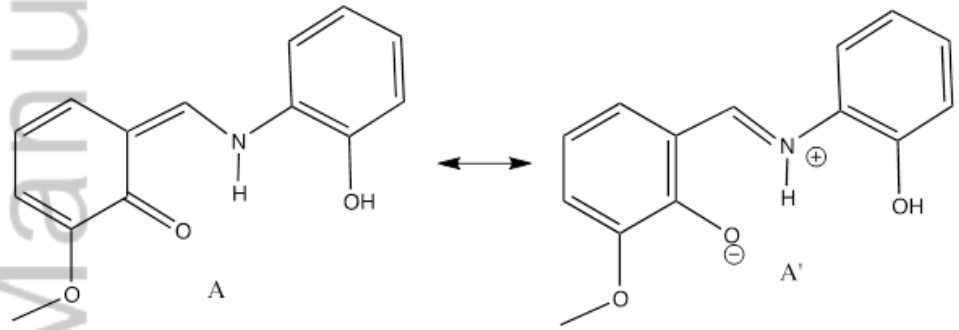

AOC_4233_F2.TIF

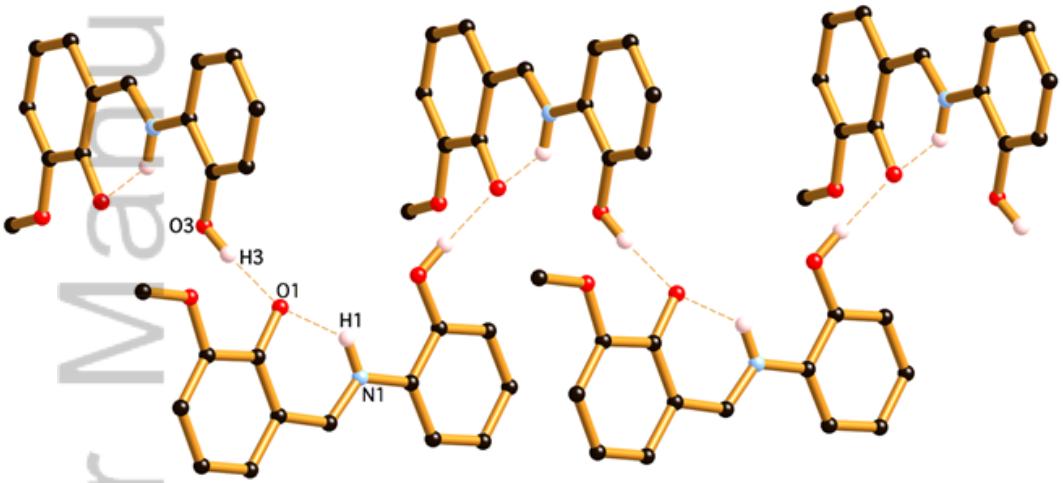

AOC_4233_F3.TIF

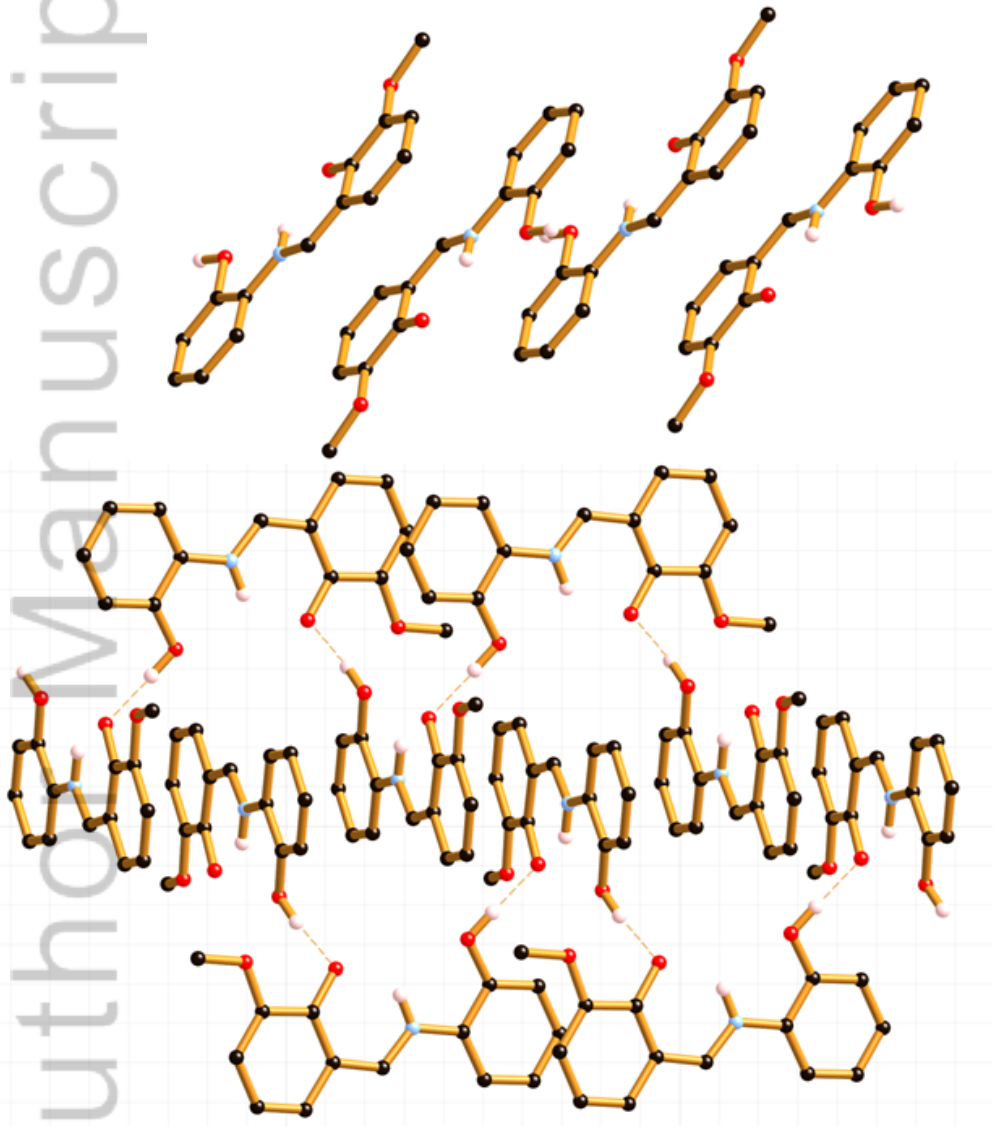

AOC_4233_F4.TIF

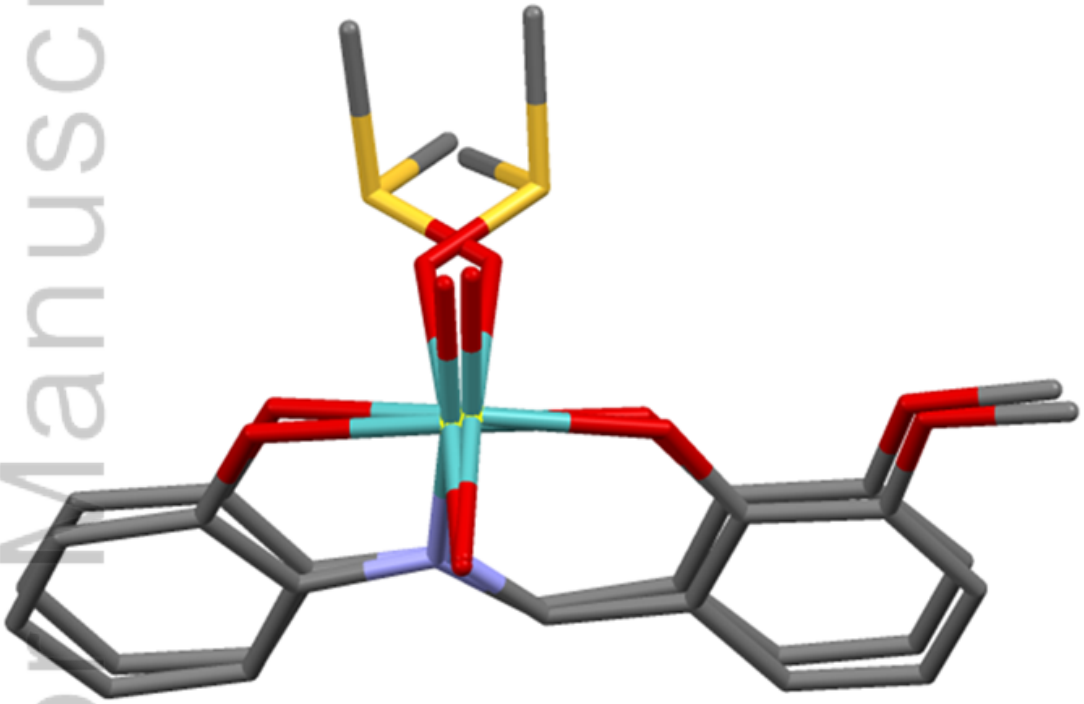

AOC_4233_F5.TIF

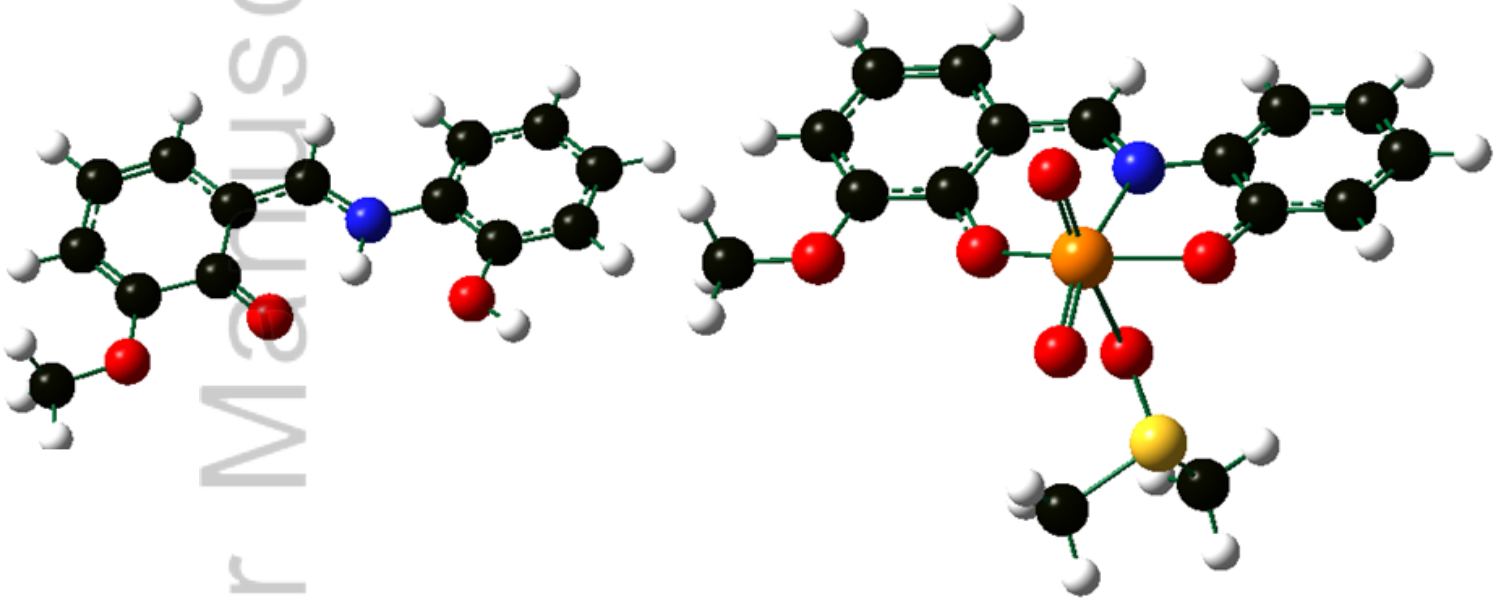

AOC_4233_F6.TIF

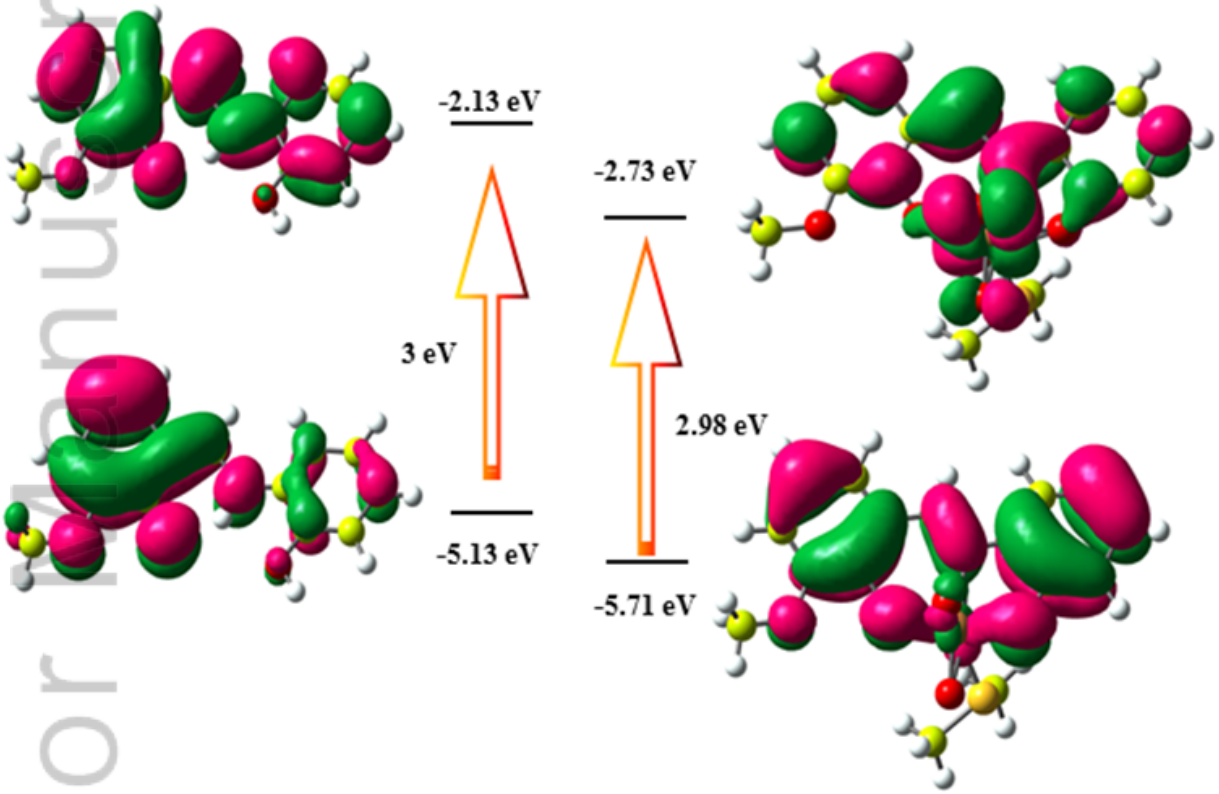

AOC_4233_F7.TIF

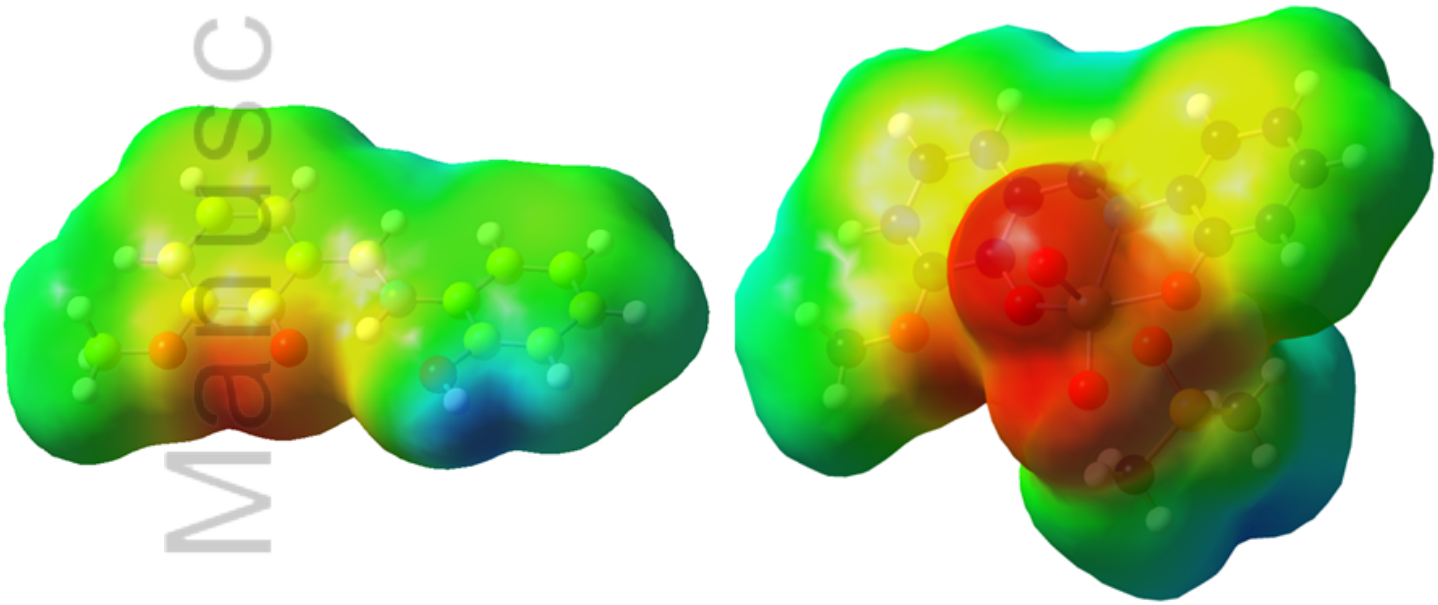

AOC_4233_F8.TIF

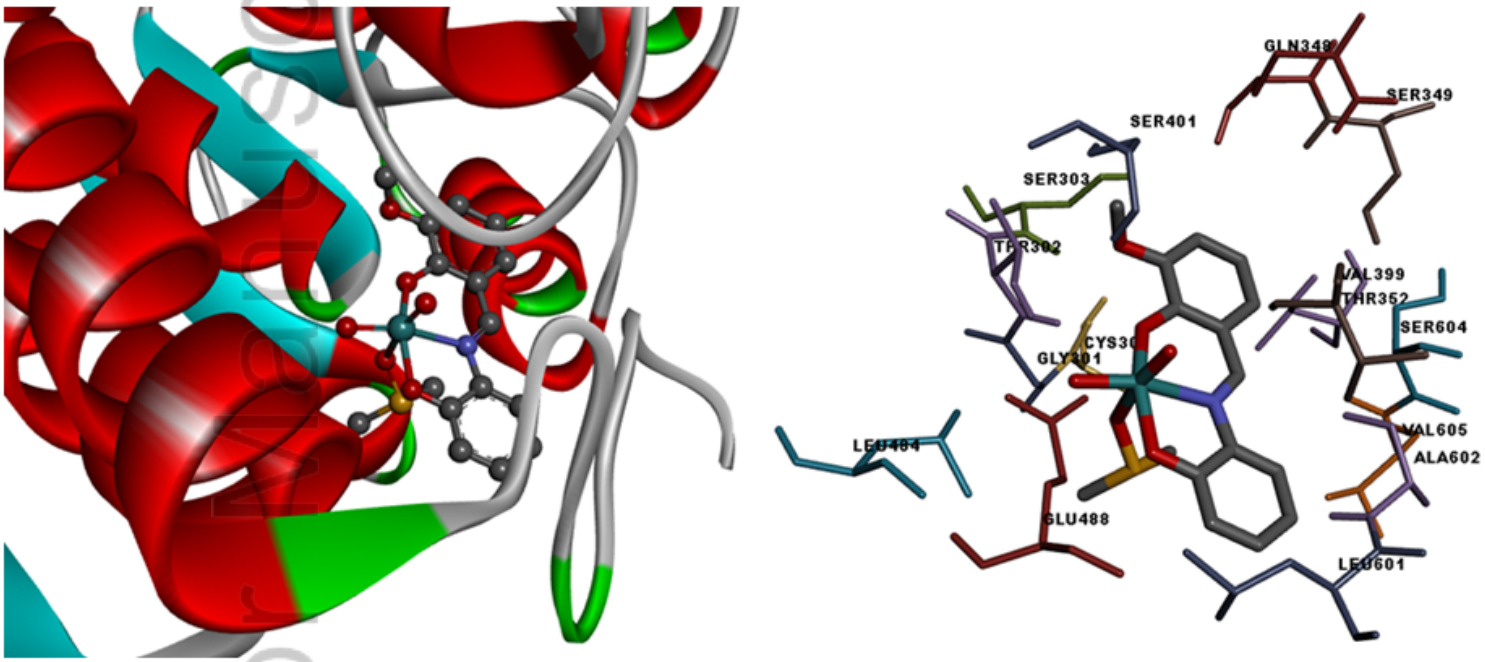

AOC_4233_F9.TIF